Tellus (1996), 48A, 272–289
Printed in Belgium – all rights reserved


TELLUS
ISSN 0280–6495

# Semi-prognostic tests of a new cumulus parameterization scheme for mesoscale modeling

By WEN-YIH SUN and PATRICK A. HAINES[1,*], *Department of Earth & Atmospheric Sciences, Purdue University, West Lafayette, Indiana 47907, USA*

(Manuscript received 24 May 1994; in final form 26 June 1995)

ABSTRACT

A new cumulus parameterization scheme is developed, discussed, and tested. 3 sizes of clouds: small, medium and large are allowed by this scheme; they crudely represent a spectrum of clouds and all 3 sizes of cloud may exist at any given time. All clouds are based on a quasi-one-dimensional cloud model that has been shown to deliver mass, moisture and heat fluxes comparable to those calculated by a 3-dimensional convective cloud model at the mature stage of a modeled convective storm. The radus of the largest cloud is twice that of the medium-sized cloud which is, in turn, twice that of the smallest cloud. The largest cloud may also have a saturated downdraft that can penetrate to the ground. In order to close the relation between the cloud and grid scales, 3 closure relations are imposed. Together, they yield a unique solution of the cloud population at any given time. In the first 2 constraints, both the convective and grid scale mass and moisture budgets are linked. Of the possible cloud sets that satisfy both the mass and moisture constraints, we choose the one that produces the fastest rate of heating from integrating the individual cloud heating rates over the possible cloud sets and over the cloud depths. The scheme is tested semi-prognostically with Sesame V storm-scale analyses during a period in which the precipitation was almost exclusively convective in nature (2000 GMT to 2300 GMT on 20 May 1979). The comparison between observed grid scale and cumulus parameterization diagnosed heating and drying rates is quite good. This is true for both individual grid points and the convectively active area as a whole.

## 1. Introduction

The importance of cumulus convection to mesoscale convective systems (MCSs) has been clearly and firmly established in both observational (Ogura and Chen, 1977; Fankhauser, 1969; Fuelberg et al., 1986) and modeling (Zhang and Fritsch, 1986; Zhang and Gao, 1989) studies. These studies show that prerequisites to the development of these systems include mesoscale areas of low-level mass and moisture convergence. Once initiated, cumulus convection provides very strong moisture, heat, and momentum feedbacks to the original circulations that rapidly intensify and often modulate them. The study by Fankhauser (1969) and the study by Ogura and Chen (1977) both show that the atmosphere responds to the feedbacks by developing a strong mesoscale overturning extending throughout the depth of the troposphere. This can increase the low-level mass and moisture convergence in a constructively interactive manner. Meanwhile, due to inability to completely portray and observe both the cumulus clouds, the MCS, and its environment, our understanding of their interaction remains inadequate.

Hydrostatic numerical prediction models are widely used in both research and operational prediction and will continue to be utilized for quite some time. It is always necessary to parameterize the effects of deep cumulus in such models

[1] Current Affiliation, Department of Meteorology, Arrhenius Laboratory, Stockholm University, S-106 91 Stockholm, Sweden.
* Corresponding author.

(Molinari and Dudek, 1992), and because the feedbacks are so important to the development of MCSs, the parameterization is crucial. No generally acceptable method of cumulus parameterization for mesoscale systems exists. Thus, there is a continuing need for improved accounting of the effect of deep cumulus in them; moreover, this is also true for fine scale non-hydrostatic model simulation employing grid nesting or adaptive strategies since it is still necessary to use cumulus parameterization in the more coarsely gridded regions of their computational domains.

Cumulus parameterization has received significant attention since cumulus clouds were identified as the primary energy source of the tropical cyclone (Charney and Eliassen, 1964). At first, most attention was devoted to tropical sytems and larger scale modeling. Several basic approaches of cumulus response to the large scale forcing have been developed (Arakawa and Schubert, 1974; Kuo, 1965; Kuo, 1974; Ooyama, 1971) and have exhibited considerable success in the simulation of tropical systems or with large scale systems (Betts, 1986). The validity of the larger scale parameterizations becomes more and more questionable when the horizontal length scale of the mesoscale system is much less than that of the radius of deformation, $R'$, (Frank, 1983; Weissbluth and Cotton, 1993).

Because the length scale of many mid-latitude MCSs is less than $R'$, the feedback in them occurs partly or primarly through the divergent wind field, making a quasi-equilibrium between generation of potential energy by the inertially large scale flow and its consumption by the MCS less likely. Reflecting this viewpoint, it has been proposed that potential energy is rapidly consumed by convective systems (Fritsch and Chappell, 1980; Kreitzberg and Perkey, 1976); however, Grell et al. (1991) and Grell (1993) show that quasi-equilibrium appears to hold in the mesoscale cases they studied. Suprisingly, when both approaches were applied to the same case (Grell, 1993), the results are quite similar. How can two seemingly different approaches give nearly the same result? We feel that this must be situation-dependent so that in other situations either quasi-equilibrium or rapid consumption of potential energy alone is appropriate but not both. For example, the Ogura and Chen (1977) study of a squall line shows that the potential instability that originally existed below 500 mb at 1430 CST prior to the squall line had been partially released by 2030 CST and was confined to a thin layer between 750 mb and 850 mb on the warm air side. The first radar echoes appeared at 1600 CST, a nearly continuous line of convection was formed by 1830 CST, and the line became disorganized after 2000 CST. The potential energy was destroyed partially by the convective heating, and partially by moisture redistribution as most of the troposphere in proximity to the MCS was moistened. Apparently, in this case, the upward moisture transport of the overturning was greater than the convective drying and, combined with the warming, quickly removed much of the potential energy possibly leading to the rapid demise of the MCS. In other situations, however, the convective drying may prevail resulting in a considerably slower diminution of the potential energy and a greater likelihood of attaining a quasi-equilibrium. Without identifiable precursors to indicate the rate at which potential energy will be consumed in a MCS or whether quasi-equilibrium will be attained, it is likely that both the quasi-equilibrium and rapid consumption of potential energy assumptions are insufficiently general closures for parameterization of convection on the mesoscale.

As viewed here, cumulus parameterization is a 3-part problem; all must be addressed. The 1st is to determine when and where convection occurs. The 2nd is to determine, once convection has been initiated, the rate of its activity in terms of the large scale environment. The 3rd is to determine the vertical distribution of the activity and the nature of its feedback to te grid scale. Even if all 3 parts of the problem are perfectly treated, there is no guarantee that a numerical model will respond to the diagnosed feedback in the same manner as the atmosphere does for a real system. The initiation, location, and vertical distribution of convective activity is discussed by Haines and Sun (1994) hereafter HS, but a closure relation for the rate of convective activity in terms of the grid scale is still required.

In the closure for the cumulus parameterization scheme (CPS) presented here, grid scale and net convective mass fluxes are equated at the cloud base level (Brown, 1979; Frank and Cohen, 1987; Song and Pielke, 1988). In this way, the model is free to respond to the effects of the convection in a manner that is hopefully similar to that of the real atmosphere. The mass flux relation is complicated by downdrafts and between cloud subsidence. The usual approach has been to specify a fixed relation between updraft and downdraft mass fluxes; instead, we allow the downdraft mass flux to be a function of the ambient conditions. Ostensibly this only devolves the closure issue to that of determining the downdraft mass flux without any reduction in the uncertainties; however, by conjunctive use of the moisture budget below cloud base discussed below, we reduce the uncertainty. This latter moisture relation avoids the problems of closures that are based on the vertically-integrated moisure budget.

In the CPS presented here, 3 convective cloud sizes may exist at any given time: large, medium, and small. Together, they crudely represent a spectrum of clouds providing the CPS flexibility to address the temporal evolution of MCSs in which cloud sizes evolve with time. It should be noted that the number of large convective clouds permissible within a meso-$\beta$ scale grid area is very limited, so a true spectrum of clouds at such resolution is unlikely. Without a true spectrum of cloud sizes, it is also unlikely to produce a realistic vertical distribution of mass, moisture and heat fluxes using simple entraining plume models. On the other hand, if the clouds are small and numerous so that a spectrum is able to satisfy the grid scale budgets, then their mass and moisture fluxes in the upper troposphere will likely be too small because their relatively large entrainment rates make them too shallow.

While the number of clouds of each size is initially unknown, the entire set must satisfy the mass and moisture constraints mentioned above. To complete the picture, in accordance with linear stability, we assume that the extant set of clouds provides the maximum rate of heating when integrated over the cloud depths of possible cloud sets. This is discussed further in Section 2. The result is a very useful diagnosis of the convective activity at any given time consistent with the grid scale forcing.

An additional advantage of the CPS described here is its employment of the new HS cloud model that gives mature storm stage mass, moisture and heat fluxes that compare reasonably well to those given by the Schlesinger 3-D convective cloud model for both sheared and non-sheared environments. In addition, in preliminary comparisons, it replicated the mass fluxes in GATE updrafts as reported by Zipser and LeMone (1980). Soong and Ogura (1977) pointed out that simple entraining plume models are incapable of replicating these fluxes. We therefore have confidence that the effects of the cumulus activity diagnosed by the CPS are distributed correctly in the vertical with consequent advantages in the feedback to the grid scale. The details about the closure, its feedback to the grid scale, and its testing are the concerns of the remainder of this article.

In Section 2, the cumulus parameterization is described and discussed. The semi-prognostic testing of the CPS and its discussion appears in Section 3. Finally, this work is summarized in Section 4. Haines (1992) incorporated this CPS in the Purdue mesoscale model (Sun and Chern, 1993; 1994) to study convection during the fourth period of the Severe Environmental Storms and Mesoscale Experiment (SESAME IV).

## 2. Formulation of the cumulus parameterization

Brown (1979), assumed that the net convective vertical mass flux, $M_c$, at cloudbase is related to the grid scale vertical mass flux, $\bar{M}$, as,

$$M_c = B\bar{M}, \tag{2.1}$$

where $B$ is a constant which if greater than 1 implies subsidence between convective clouds. At the meso-$\beta$ scale ($20\ \text{km} < dx < 50\ \text{km}$), a fairly close relation between the grid scale and net convective scale mass fluxes at the cloud base level has also been proposed by Song and Pielke (1988) and Frank and Cohen (1987). This close relation is complicated by the downdrafts that many convective storms have and the vertical mass flux that may occur between storms. The above investigators fixed or restricted the relation between up and downdraft mass fluxes at cloud base partly to prevent the downdraft mass fluxes from exceeding those of the updraft and partly due to inability to calculate the downdraft fluxes. Because the CPS cloud model used here calculates net convective mass fluxes at cloud base that are in reasonable agreement with those from the Schlesinger model at the mature storm stage, we believe that we can calculate net convective mass fluxes at cloud base that provide more information than the fixed relation used by the other investigators. Frank and Cohen used a cloud base subsidence mass flux that is 20% of the updraft mass flux; however, we chose to set $B = 1.0$ because there is neither sufficient observational basis nor the requisite physical understanding by which to specify a $B$-value other than 1.0. Furthermore, the limited observational and modeling evidence shows that only precipitation-associated downdrafts systematically reach the surface and that both penetrative and regional compensating downdrafts are mainly confined to above the cloud base level (Knupp, 1987; Soong and Ogura, 1977). Thus, as mentioned by Frank and Cohen, the more critical value is downdraft mass flux. As shown in Knupp (1987), this can be more than 50% of the updraft value at cloud base.

The grid scale vertical mass flux is expressible as,

$$\bar{M} = \rho \bar{w} A, \tag{2.2}$$

where $\bar{w}$ is the grid scale vertical velocity as cloud base, $A$ is the grid scale area, and $\rho$ is the density at the cloud base level. The net convective mass flux consists of updraft $M_u$ and downdraft $M_d$ components as

$$M_c = M_u + M_d. \tag{2.3}$$

Equating grid scale and net convective mass fluxes gives,

$$\bar{M} = M_c = M_u + M_d. \tag{2.4}$$

Because, as mentioned above, $M_d$ can vary from zero to perhaps as much or more than one-half of the updraft flux, from 2.4, the corresponding variation in the amount of updraft mass flux may be as much as 100% or more. This is why we are more concerned with establishing the amount of downdraft mass flux than the between cloud subsidence for a given situation.

The net convective mass flux is a summation of updraft mass fluxes of the three cloud sizes plus the downdraft mass flux of the large clouds (only large (type 3) clouds are assumed to have penetrative downdrafts),

$$M_c = \sum_i N_i A_{ui} w_{ui} \rho_{ui} + N_3 w_{D3} A_{D3} \rho_{D3}, \tag{2.5}$$

where $N_i$ is the number of and $A_{ui} w_{ui} \rho_{ui}$ is the updraft mass flux of the $i$th-size cloud.

Organized deep convection requires considerable moisture convergence in order to sustain its heavy moisture consumption. Although the rate of condensation in MCSs is reasonably well correlated to the grid scale moisture supply, this relation is less firm than it is for the mass fluxes as there may be an appreciable time lag between the start of moisture convergence and the onset of the convection (Kuo and Anthes, 1984) and, once started, the convection may consume the available moisture at a rate in excess its supply.

The portion of the moisture supply that is condensed and then evaporated is difficult to establish and has a direct bearing on the level of downdraft activity. A wind shear-precipitation efficiency relation (Marwitz, 1972; Foote and Fankhauser, 1973) has been used by several investigators (Fritsch and Chappell, 1980; Grell, 1993; Molinari and Corsetti, 1985) to govern the downdraft activity, however, Fankhauser's (1988) results support indications from numerical models that this relation is likely more complicated than a simple inverse relation with wind shear.

The uncertainty in the mass-flux closure can be reduced when the convective moisture transports at the cloud base level are related to the moisture budget below cloud base similar to the treatment shown in Tiedtke (1989). This is because the saturation mixing ratio in a cold downdraft is less than it is in the updraft. Thus, the amount of the net convective vertical moisture flux at the cloud base level made up by that in the updraft is greater than it is for the mass flux, and this difference increases for stronger and colder downdrafts that presumably provide relatively larger mass fluxes. The result is a relation between the grid scale vertical moisture flux, the net convective moisture flux, the possible moisture transfer by between cloud mixing and the integrated amount of evaporation of precipitation below cloud base.

One part of the moisture budget that was ignored here is the moisture flux from the earth's surface. One reason is the difficulty of estimating this in this study. Furthermore, for a humid boundary layer over a 90-min period, as was the case here and shown below, this is relatively small in comparison to the other parts of the moisture budget. For much longer time periods and/or less humid boundary layers this will not be the case. In practice, when coupled with a mesoscale model, the surface fluxes are available from the model's boundary layer treatment. Taken together, the mass and moisture constraints offer a better relation between the convective and grid scales than either alone.

We avoid using the integrated horizontal moisture convergence and its unknown relation to the precipitation rate by focusing on the moisture budget below cloud base, which is less sensitive to these problems. Beginning with conservation of moisture,

$$\frac{\mathrm{d}q}{\mathrm{d}t}=S_q, \tag{2.6}$$

where $S_q$ denotes sources and sinks of water vapor. Writing 2.6 in flux form along with condensation, $C$, and evaporation, $e$, of water substance for the water sources and sinks yields,

$$\frac{\partial q}{\partial t}+\nabla\cdot V_q+\frac{\partial(\omega q)}{\partial p}=C-e. \tag{2.7}$$

We partition the variables into grid scale averages denoted by an overbar ($^-$) and perturbations denoted by a prime ($'$) as

$$\begin{aligned} q&=\bar{q}+q', \\ V&=\bar{V}+V', \\ \omega&=\bar{\omega}+\omega', \end{aligned} \tag{2.8}$$

and average all quantities over the grid scale. The result is,

$$\frac{\partial\bar{q}}{\partial t}+\nabla\cdot\bar{V}\bar{q}+\frac{\partial\bar{\omega}\bar{q}}{\partial p}=\overline{C^*}-\frac{\partial\overline{\omega'q'}}{\partial p}, \tag{2.9}$$

where $C^*$ includes both condensation and evaporation. Eq. (2.9) follows from Anthes (1977) where it was assumed that $\overline{q'}=0$, $\bar{\bar{q}}=\bar{q}$, $\nabla\cdot\overline{V'q'}=0$, and that a number of other terms such as $\overline{\omega'\bar{\chi}}=0$ or $\overline{\bar{\omega}\chi'}=0$. Schlesinger (1990, 1994) shows that neglect of the latter terms may be inappropriate, however, his results need to be confirmed on a wider variety of environments. Following Anthes (1977) and generalizing for a population of differently sized clouds, the covariance on the right hand side of 2.9 is:

$$\overline{(\omega'q')}=\frac{A}{(1-A)}(\bar{\omega}_{\mathrm{c}}^{\mathrm{c}}-\bar{\omega})(\bar{q}_{\mathrm{c}}^{\mathrm{c}}-\bar{q}), \tag{2.10}$$

where $A$ is the total area occupied by convective clouds,

$$A=\sum_{i=1}^{3}a_iN_i,$$

in which $a_i$ and $N_i$ are respectively the area and number of $i$th-size clouds, and $\bar{\omega}_{\mathrm{c}}^{\mathrm{c}}$ and $\bar{q}_{\mathrm{c}}^{\mathrm{c}}$ are the average vertical velocity and the average water vapor mixing ratio, respectively, in the convective clouds or,

$$\bar{\omega}_{\mathrm{c}}^{\mathrm{c}}=\sum_{i=1}^{3}a_iN_i\bar{\omega}_{\mathrm{c}i}^{\mathrm{c}}/A,$$

$$\bar{q}_{\mathrm{c}}^{\mathrm{c}}=\sum_{i=1}^{3}a_iN_i\bar{q}_{\mathrm{c}i}^{\mathrm{c}}/A;$$

$\bar{\omega}_{ci}^{\mathrm{c}}$ and $\bar{q}_{ci}^{\mathrm{c}}$ are the average vertical velocity and water vapor mixing ratio, respectively, in an $i$th-size cloud.

Integrating (2.9) vertically from the surface to cloud base level yields,

$$\underbrace{-\frac{1}{g}\int_{P_{\mathrm{sfc}}}^{P_{\mathrm{LCL}}}\frac{\partial\bar{q}}{\partial t}\,\mathrm{d}p}_{A}\;\underbrace{-\frac{1}{g}\int_{P_{\mathrm{sfc}}}^{P_{\mathrm{LCL}}}\nabla\cdot\bar{V}\bar{q}\,\mathrm{d}p}_{B}$$

$$\times\underbrace{-\frac{1}{g}\int_{P_{\mathrm{sfc}}}^{P_{\mathrm{LCL}}}\frac{\partial(\bar{\omega}\bar{q})}{\partial p}\,\mathrm{d}p}_{C}=\underbrace{-\frac{1}{g}\int_{P_{\mathrm{sfc}}}^{P_{\mathrm{LCL}}}\overline{e^*}\,\mathrm{d}p}_{D}$$

$$\times\underbrace{+\frac{1}{g}\int_{P_{\mathrm{sfc}}}^{P_{\mathrm{LCL}}}\frac{\partial\overline{(\omega'q')}}{\partial p}\,\mathrm{d}p}_{E}. \tag{2.11}$$

When integrated over the cloud depth, term $A$ is the water storage. Although many studies have found it to be relatively small (Fuelberg et al., 1986), McNab and Betts (1978) found that cloud storage was important for their developing class of convection where the convection changed rapidly from weak to moderate or precipitating. When integrated over the below cloud layer, as is done here; however, the change in storage as compared to the horizontal moisture convergence (term $B$) should almost always be small. Therefore, we neglect term $A$. Because eq. (2.11) is applied only to the below cloud base, we need not be concerned with condensation; hence, only evaporation is included in term $D$ for changes of state.

Evaluating (2.11) above, making use of (2.10) and using

$$\bar{\omega} = \sum_{i=1}^{3} a_i N_i \overline{\omega_{ci}^{c}}$$

at cloud base, we find that the net convective moisture flux at cloud base is,

$$Q_c = \sum_{i=1}^{3} a_i N_i \overline{\omega_{ci}^{c}}\,\overline{q_{ci}^{c}}. \tag{2.12}$$

This may be expressed as,

$$Q_c = -\int_{p_{sfc}}^{p_{LCL}} \nabla \cdot \bar{V}\bar{q}\,dp + -\int_{p_{sfc}}^{p_{LCL}} \bar{e}^*\,dp - (\overline{\omega' q'})_{sfc}. \tag{2.13}$$

Eq. (2.13) is similar to Tiedtke (1989). The 3 terms on the right-hand side of (2.13) are the horizontal moisture convergence vertically-integrated from the surface to cloud base, the evaporation of precipitation below cloud base, and the surface moisture flux, respectively. The evaporation is discussed in HS. When the CPS is included as part of a mesoscale model package, the surface moisture flux is available as part of the surface physics. For this study; however, this was not the case, so it was estimated by the bulk aerodynamic method and found to be much less than the vertically-integrated horizontal moisture convergence during the period of intense convective activity. The surface moisture flux was estimated to have been about $1 \times 10^{-4}$ kg m$^{-2}$ s$^{-1}$ in the storm-scale region based on a wind speed of 5 m s$^{-1}$, a drag coefficient of 0.005 and a moisture difference between the ground and the wind measurement level of 0.003 kg kg$^{-1}$. Meanwhile, the horizontal moisture convergence between the surface and 900 mb at this time (Fuelberg et al., 1986) was greater than $1 \times 10^{-3}$ kg m$^{-2}$ s$^{-1}$.

In a manner similar to that for the moisture budget, the rate of heating at any level due to an $i$th-size cloud is,

$$\frac{\partial \theta_i}{\partial t} = \frac{L}{c_p}\left[\langle C_i^* \rangle - \langle e_i^* \rangle\right] - \frac{\partial(\overline{\omega' \theta'})}{\partial p}, \tag{2.14}$$

where $\langle C_i^* \rangle$ and $\langle e_i^* \rangle$ are, respectively, the rates of condensation and evaporation and the vertical eddy flux of heat is:

$$\overline{(\omega' \theta')} = \frac{A}{(1-A)}(\bar{\omega}_c^c - \bar{\omega})(\bar{\theta}_c^c - \bar{\theta}), \tag{2.15}$$

where all the variables are defined as in 2.10 except that $\bar{\theta}_c^c$ is the average potential temperature for all the convective clouds at a given level,

$$\bar{\theta}_c^c = \sum_{i=1}^{3} a_i N_i \bar{\theta}_{ci}^c / A.$$

$\bar{\theta}_{ci}^c$ is the average potential temperature at a given level in an $i$th-size cloud. All the terms on the right hand side of eq. (2.14) are readily calculated for an $i$th-size cloud with the HS cloud model. Compressional heating due to subsidence outside the visible cloud does not explicitly appear in (2.14), but Kuo (1974) clearly demonstrated that this heating is implicitly incorporated in this formulation.

As a convective system evolves, observations show that the grid scale mass and moisture fluxes increase considerably. At the same time, the cloud spectrum may evolve from a large number of small to medium sized clouds to a small number of larger clouds. This latter set of clouds may have arisen from cloud mergers. From a linear stability standpoint, the cloud(s) with the highest rate of heat production and consequent largest external subsidence flows are expected to dominate and extirpate their companions that have a slower rate of heat production. As an example, Sun (1984) using a linearized two-dimensional model with condensational heating for ascending motion and no heating for descending motion, showed that small weak rainbands are dissipated by the subsidence warming emanating from stronger rainbands. As a result, the eventual horizontal length scale of simulated rainbands was quite different from the initial model conditions, but consistent with observations of the Baiu front and the 3–4 April 1974 squall lines in the United States. Therefore, to complete the closure between the crude spectrum of clouds in this parameterization, that also satisfies both equations (2.1) and (2.13), we assume that the set of clouds extant at any given time ($N_1$ = number of smaller clouds, $N_2$ = number of medium clouds, $N_3$ = number of large clouds) produces the maximum rate of heating when integrated over the cloud depths of all clouds,

$$\sum_{i=1}^{3} N_i \int_{P_{\mathrm{LCL}}}^{P_{\mathrm{ETL}}} \frac{\partial \theta_i}{\partial t} A_i \, \mathrm{d}p = H, \tag{2.16}$$

where $H$ = heat maximum, $P_{\mathrm{LCL}}$ refers to the pressure at cloud base, and $P_{\mathrm{ETL}}$ to the pressure at cloud top.

Assuming that a set of 3 cloud types exists, we may write equations (2.4), (2.13), and (2.16) as

$$N_1 M_1 + N_2 M_2 + N_3 M_3 = \bar{M}, \tag{2.17}$$

$$N_1 Q_1 + N_2 Q_2 + N_3 H_3 = \bar{Q}, \tag{2.18}$$

$$N_1 H_1 + N_2 H_2 + N_3 H_3 = \max, \tag{2.19}$$

where $\bar{Q}$ represents the terms on the right hand side of eq. (2.13), $M_1$ and $Q_1$ represent respectively the updraft fluxes of mass and moisture in small clouds, $M_2$ and $Q_2$ represent respectively the updraft fluxes of mass and moisture in medium size clouds, $M_3$ and $Q_3$ represent respectively the net mass and moisture fluxes from both updrafts and downdrafts in large size clouds, and,

$$H_i = \int_{P_{\mathrm{LCL}}}^{P_{\mathrm{ETL}}} \frac{\partial \theta_i}{\partial t} \rho_{\mathrm{u}i} A_{\mathrm{u}i} \, \mathrm{d}p. \tag{2.20}$$

The 3 constraints represented by eqs. (2.17), (2.18), and (2.19) enable a unique solution for $N_1$, $N_2$, and $N_3$ to be obtained. For a given convective environment, a number of combinations of cloud types one through three can satisfy eqs. (2.17) and (2.18); however, only one of these combinations also gives the maximum rate of heating using (2.19). This particular combination is identified by examining all the possible combinations that satisfy the mass and moisture constraints and finding the one that maximizes the heating rate.

## 3. Semi-prognostic testing of the CPS with Sesame V data

During the 5th observing period of the 1979 AVE-SESAME experiment (SESAME V), a meso-$\beta$ scale array of 19 radiosonde stations, 7 Doppler radars, 79 automated surface stations, the National Severe Storms Laboratory's WSR-57 digitized radar and an instrumented television tower made observations in western and central Oklahoma and the eastern Texas panhandle (Alberty et al., 1979). The average spacing of the radiosonde locations is approximately 75 km which is similar to that made by the National Severe Storms Laboratory (NSSL) radiosonde array during the 1960s and 1970s; however, the NSSL network had only 9 stations. Only a very few of the NSSL cases have been utilized to study the budgets of mesoscale convective systems. Radiosonde observations were made every 3 h between 1100 GMT on 20 May to 1100 GMT on 21 May 1979 and special radiosonde observations were made at 2130 GMT on 20 May. Thus, data are available at 90-min intervals from 2000 GMT to 2300 GMT; this period coincides with the most intense and widespread occurrence of convective activity within the storm scale array during SESAME V.

### 3.1. *Objective analysis*

Most of the soundings are representative of the mesoscale environment and many extend well into the upper troposphere documenting the events of SESAME V quite well. The reader is referred to Fuelberg and Printy (FP) (1983) who thoroughly describe the careful initial checking of the radiosonde data.

The data were objectively analyzed by FP onto a 15 by 13 storm-scale analysis grid using a Barnes type procedure. The horizontal spacing of this grid is 25 km. Data were analyzed at the surface (at about 950 mb in western Oklahoma) and at 50 mb intervals from 900 to 150 mb. There were insufficient data at 100 mb to make analyses. According to FP, the final analysis fields have response values that are about 32% of originally resolved amplitudes for wavelengths of 150 km and 82% for wavelengths of 225 km. Centered finite differences were employed by FP in calculating horizontal derivatives. Kinematic vertical velocities ($\omega$) were calculated, but as is often the case, their values at the highest levels appeared excessive. Therefore, $\omega$ values were adjusted to zero at the 150 mb level. The corresponding modifications to horizontal divergence were a linear function of pressure. Even after this modification, at several grid locations, $\omega$'s corresponding to vertical velocities in excess of $1 \mathrm{~m\,s^{-1}}$ are noted in the middle and upper troposphere during the 2000 and 2300 GMT time period.

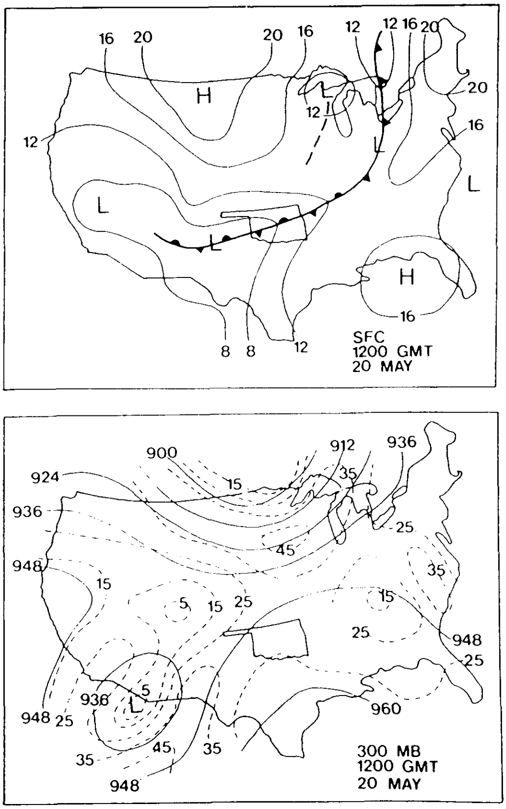


*Fig. 1.* National Meteorological Center surface analysis (top panel) and 300 mb analysis (bottom panel) for 1200 GMT on 20 May 1979. Isotachs (dashed) are in m s$^{-1}$ (after Fuelberg and Printy, 1983).

### *3.2. Synoptic and mesoscale conditions*

The surface synoptic conditions over the Great Plains and elsewhere at 1200 GMT on 20 May are shown in the top panel of Fig. 1. A cold front extended southwestward from the Great Lakes to Oklahoma where it became stationary. The stationary front extended westward into New Mexico. High pressure prevailed over the northern Rocky Mountain and Great Plains states. At 300 mb as shown in the bottom panel of Fig. 1, a cut-off low was located over Arizona while a short wave trough was positioned over the upper Middle West. Winds in the upper troposphere over Oklahoma at this time and throughout the SESAME V period were less than 35 m s$^{-1}$.

Small radar echoes were first noted along the stationary front in Texas at 1700 GMT on 20 May.

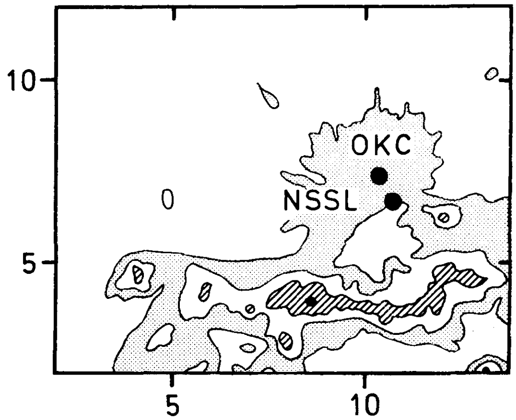


*Fig. 2.* Composite radar analysis for 2130 GMT on 20 May 1979. The contours are for Digital Video Integrator Processor levels 1 through 6. Level 1 (DVIP > 30 dbz) is shaded, level 2 is whitespace bounded by level 1, and level 3 and above is cross-hatched. The storm-scale analysis region shown by the heavy dark rectangle. The numbers 5 and 10 along the south and west sides of the rectangle indicate the location of the 5th and 10th grid points in the storm scale analysis. (after Watson et al., 1988).

The convective activity gradually became more intense and widespread so by 2130 GMT, as shown in Fig. 2, it covered much of the southern half of the storm-scale analysis area. For reference purposes, the rectangular outline of the innermost 13 x 11 gridpoint region of the storm-scale grid has been superimposed on both Figs. 2, 3. Also shown along the southern and western boundary of this

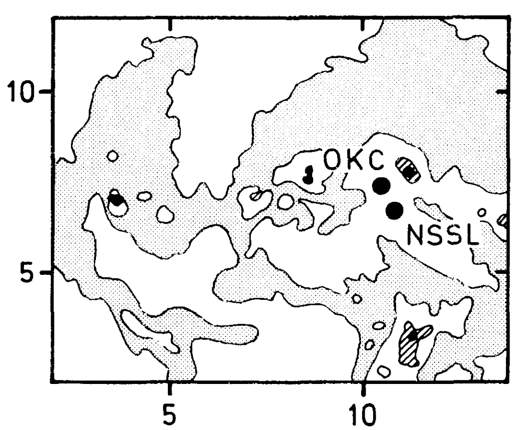


*Fig. 3.* As for Fig. 2 but for 2330 GMT on 20 May 1979.

rectangle, are tick marks for the fifth and tenth grid points of this grid.

2 h later at 2330 GMT, as shown in Fig. 3, the heavy convective activity was largely confined to the southeastern quandrant of the storm-scale analysis area having moved eastnortheastward. In addition, by this time, fairly extensive areas of stable precipitation are also present.

After an additional period of 2 h at 0135 GMT (not shown), the convective activity had both abated and moved out of the storm-scale grid area. Light rain continued over Oklahoma until 0600 GMT augmenting the copious amounts that had already fallen. Widespread 24-h rainfall totals within the storm-scale area ranged upwards to and in excess of 75 mm.

As is evident from the radar observations shown in Figs. 2, 3, convective activity within the storm scale area was mainly restricted to the three hour period from 2000 GMT to 2300 GMT on 20 May. Further corroboration is that significant vertical motion extended throughout the depth of the troposphere only from 2000 GMT to 2300 GMT (Watson et al., 1988; Fuelberg and Printy, 1983). Although significant vertical motion above 600 mb persisted until 0600 GMT on 21 May, upward vertical motion below 600 mb virtually ceased at 2300 GMT. The vertical distribution of the vertical motion after 2300 GMT is consistent with the cessation of convective activity at this time and subsequent development of widespread stratiform precipitation as was observed. Watson et al. (1988) using a somewhat larger storm-scale analysis domain than FP reached similar conclusions. In addition, the latter investigators found that very little stratiform rainfall occurred in their analysis domain, that encompasses FPs, prior to 2300 GMT on 20 May 1979.

Watson et al. estimated the rain volume at half-hourly intervals in the storm-scale network on the basis of the areal coverage and type (stratiform or convective). They divided the rainfall into convective and stratiform parts on the basis of the area, and possible fluctuating, cellular, or core nature of the radar reflectivities. Convective activity within their storm-scale region began at about 1700 GMT on 20 May 1979 and increased in intensity and areal coverage until about 2130 to 2200 GMT. The increase in activity was most rapid between 1900 to 2100 GMT. After 2200 GMT, the convective rainfall within their storm-scale region subsided and finally ended at 1000 GMT on 21 May 1979. The greatest convective activity occurred between 2000 and 2300 GMT.

According to Watson et al. (1988), very little stratiform rainfall occurred until 2300 GMT, but its amount steadily increased thereafter, reaching its peak at about 0500 GMT on 21 May 1979. Their stratiform rain rate exceeded that of the convective from 0200 GMT onward and the ratio of total stratiform to total convective rainfall was 50:50. Watson et al. also concluded that about 50% of the total stratiform rain was probably due to horizontal transfer of condensate from the convective region. Thus, the latent heating associated with the stratiform rain is less than it would be if the amount of stratiform rain alone were considered; however, it appears to have constituted about 25% of the total latent heating of this case and likely was greater than that due to the convective activity after 0400 GMT on 21 May.

Most prior semi-prognostic tests have been done for an extended period (Grell et al., 1991 includes the entire 24-h period of SESAME V) thereby incorporating the effects of stratiform rainfall, so that the large scale diagnosis of heating and drying includes the effect from both convective and stratiform precipitation. In addition, averaging over the longer time period makes the neglect of radiation less acceptable. The CPS described in this paper has been designed solely to account for the effect of convection with the tacit assumption that the numerical model with which the CPS is paired will explicitly resolve and account for the stratiform rainfall. Therefore, it appears most valid to apply the semi-prognostic testing for this case, or any other case in which stratiform rainfall contributes significantly to the latent heating and effects, only when stratiform rainfall is absent or much less important than the convective rainfall or be able to remove the stratiform rain's effects from the large scale diagnoses. Fortuitously, the 90-min interval of observations made during the 2000 to 2300 GMT time period of SESAME V is when the storm scale rainfall was predominately convective in nature. This restriction on semi-prognostic testing can be lifted if the total portion of latent heating contributed by the stratiform rainfall is calculated following a procedure such as employed by Watson et al. (1988) or by using a mesoscale model with a fairly complete microphysical parameterization.

### 3.3. Procedure

The apparent heat source ($Q_1$) and the apparent moisture sink ($Q_2$) are defined (Ogura and Chen, 1977; Yanai et al., 1973) as,

$$Q_1 = \frac{\partial \bar{\theta}}{\partial t} + \nabla \cdot \bar{V}\bar{\theta} + \frac{\partial \bar{\omega}\bar{\theta}}{\partial p}, \tag{3.1}$$

$$Q_2 = -\left(\frac{\partial \bar{q}}{\partial t} + \nabla \cdot \bar{V}\bar{q} + \frac{\partial \overline{\omega q}}{\partial p}\right). \tag{3.2}$$

These represent the effects of the convective clouds on the moisture and thermal structure of the grid scale. Following Ogura and Chen (1977), the average $Q_1$, denoted as $[Q_1]$, is defined as,

$$[Q_1] = \int_{t_1}^{t_2} \left[\frac{\partial \bar{\theta}}{\partial t} + \nabla \cdot \bar{V}\bar{\theta} + \frac{\partial \bar{\omega}\bar{\theta}}{\partial p}\right] \mathrm{d}t, \tag{3.3}$$

and the average $Q_2$, $[Q_2]$ is defined as,

$$[Q_2] = \int_{t_1}^{t_2} \left[\frac{\partial \bar{q}}{\partial t} + \nabla \cdot \bar{V}\bar{q} + \frac{\partial \overline{\omega q}}{\partial p}\right] \mathrm{d}t, \tag{3.4}$$

where $t_1$ and $t_2$ are respectively the times at the beginning and end of a time period over which $Q_1$ and $Q_2$ are calculated.

The right-hand side of eqs. (3.3) and (3.4) were calculated with a finite difference approximation using the FP 25 km horizontal resolution analysis fields at the start and finish of each 90-min period. These analyses were also used to initialize the CPS at a given time. The instantaneous heating and drying rates diagnosed by the CPS were then extrapolated over a 90 minute period in order to compare to an average value of the large scale terms over the same period.

The CPS heating rate with which to compare to the result of eq. (3.3) is defined as:

$$[Q_1]_{\mathrm{cps}} = \left[\frac{L}{\pi c_{\mathrm{p}}}\left(\frac{p_{\mathrm{o}}}{p}\right)^{\kappa}(\bar{C} - \bar{e}) + \frac{\partial \overline{\omega' \theta'}}{\partial p}\right](t_2 - t_1), \tag{3.5}$$

and the CPS drying rate with which to compare to eq. (3.4) is defined by

$$[Q_2]_{\mathrm{cps}} = \left[(\bar{C} - \bar{e}) + \frac{\partial \overline{\omega' q'}}{\partial p}\right](t_2 - t_1). \tag{3.6}$$

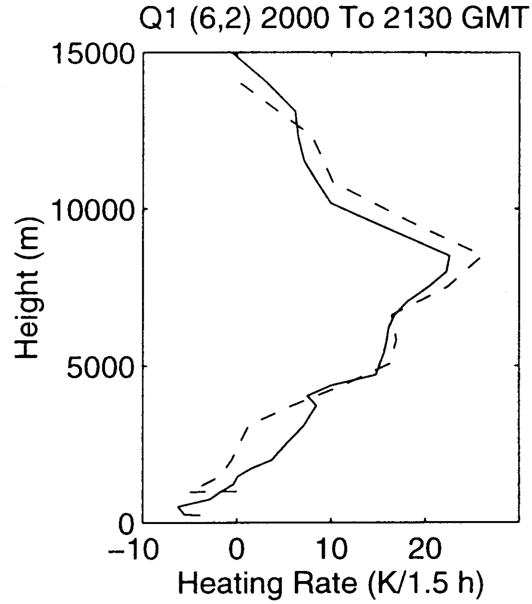


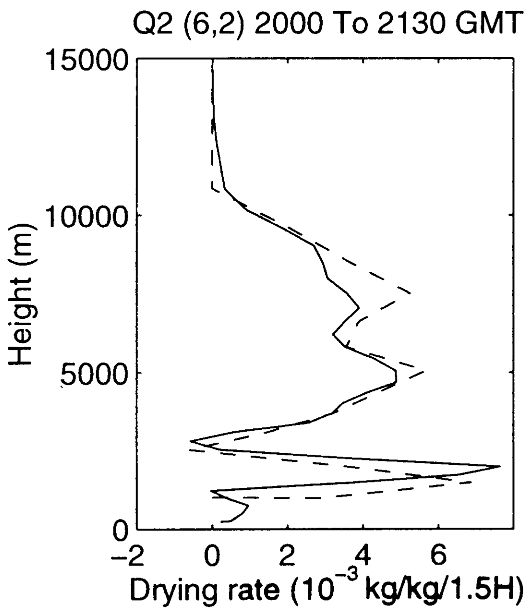


*Fig. 4.* Comparison of observed (solid) and CPS diagnosed (dashed) $Q_1$ (top) and $Q_2$ (bottom) extrapolated for a 90-min period, 2000 GMT to 2130 GMT, on 20 May 1979 for the grid point (6, 2).

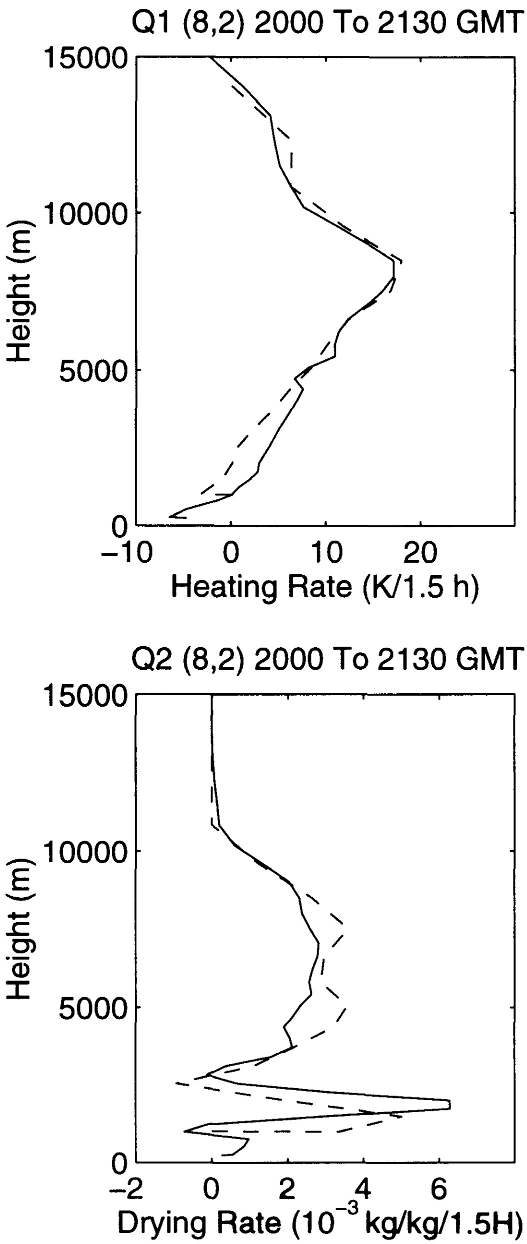


*Fig. 5.* As for Fig. 4 except for grid point (8, 2).

Numerous comparisons of the CPS diagnosed and large scale calculated values of ($Q_1$) and ($Q_2$) were made at individual grid boxes in the storm-scale analysis grid for the time period when convection was at its most intense phase (2000 GMT to 2300 GMT). A selection of these comparisons appear below. For each comparison, the particular grid point within the 15 by 13 analysis grid region and the time appears along the top edge of each figure. The ordinate for each graph is altitude and the abscissas are degrees per 90 min or kg kg$^{-1}$ per 90 min for $Q_1$ and $Q_2$, respectively. The grid scale values are labeled as the observed curves (dashed) while those diagnosed by the cumulus parameterization are labeled as the CPS curves (solid). The heating and drying rates were calculated for two 90-min time periods: 2000 GMT to 2130 GMT, and 2130 GMT to 2300 GMT.

We chose to split the comparisons at individual grid points into two types: (1) weak convective activity (maximum observed $Q_1$ less than 10 K per 90-min period); (2) strong convective activity (maximum $Q_1$ greater than 10 K per 90-min period). This distinction allows us to demonstrate that the CPS correctly diagnoses both levels of activity. Figs. 4–7 shows the $Q_1$ and $Q_2$ comparisons at a few representative grid points with strong convective activity. Figs. 4, 5 are for the time period from 2000 GMT to 2130 GMT on 20 May 1979. The $Q_1$ comparisons appear in the top panel of each figure and the $Q_2$ comparisons are in the lower panel. The convective activity at these grid points was quite intense producing the very large heating and drying rates (heating rates are as large as 20 to 30 K per 90 min or about 1.5 to 2 times as large as those calculated by Ogura and Chen (1977)) shown in these figures. As may be seen in Figs. 4, 5, in both amount and vertical structure, the CPS diagnoses compare quite closely to the observed $Q_1$ and $Q_2$ values. This continues to be the case at other convectively active grid points.

Figs. 6, 7 are representative samples of the comparisons for the second part of the intensively observed period (2130 GMT to 2300 GMT). The comparisons continue to show very good agreement between the diagnosed heating or drying and the observed values.

Figs. 8, 9 show the comparisons for grid points with weak convective activity, continue to be on the same basis as those above, and are generally good. It is noteworthy that while the vertical structures are not as well delineated as for the strong comparisons, the overall amount and distribution of heating and drying is diagnosed quite accurately. The intent of these comparisons, as mentioned above, is to demonstrate that the CPS can diagnose the effects of deep convection for all levels of convective activity.

In Fig. 10, the average $Q_1$ and $Q_2$ comparisons for the convectively active part of the lower half

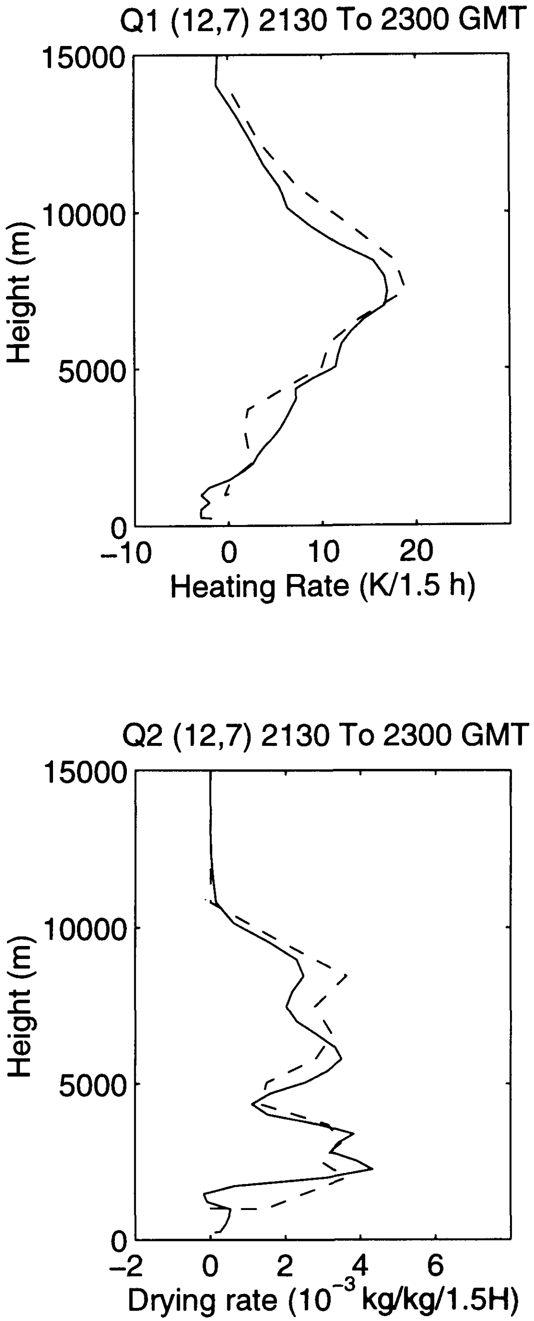


*Fig. 6.* Comparison of observed (solid) and CPS diagnosed (dashed) $Q_1$ (top) and $Q_2$ (bottom) extrapolated for a 90-min period, 2130 GMT to 2300 GMT, on 20 May 1979 for the grid point (12, 7).

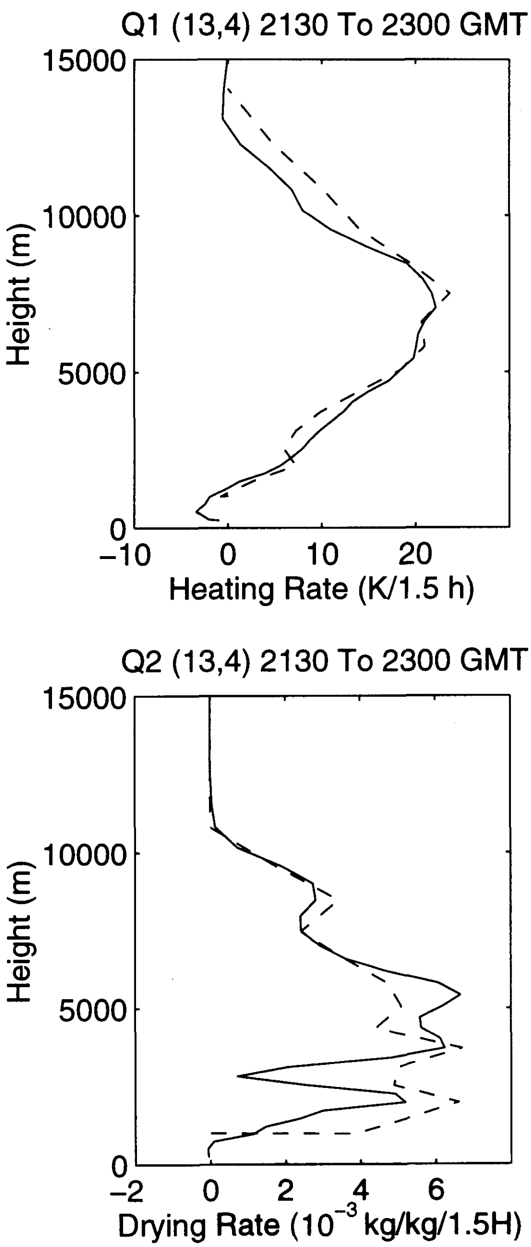


*Fig. 7.* As for Fig. 8 except for grid point (13, 4).

of the storm-scale analysis grid during the time period 2000 GMT to 2130 GMT are shown. The level of activity diagnosed by the CPS is somewhat less than observed. We attribute this to there having been an increase of activity during this time while the CPS diagnoses are based solely on the initial tendencies. Watson et al. (1988) with a similar area to that used here note an increase in activity during this time which was largely accomplished through an increase in areal coverage of

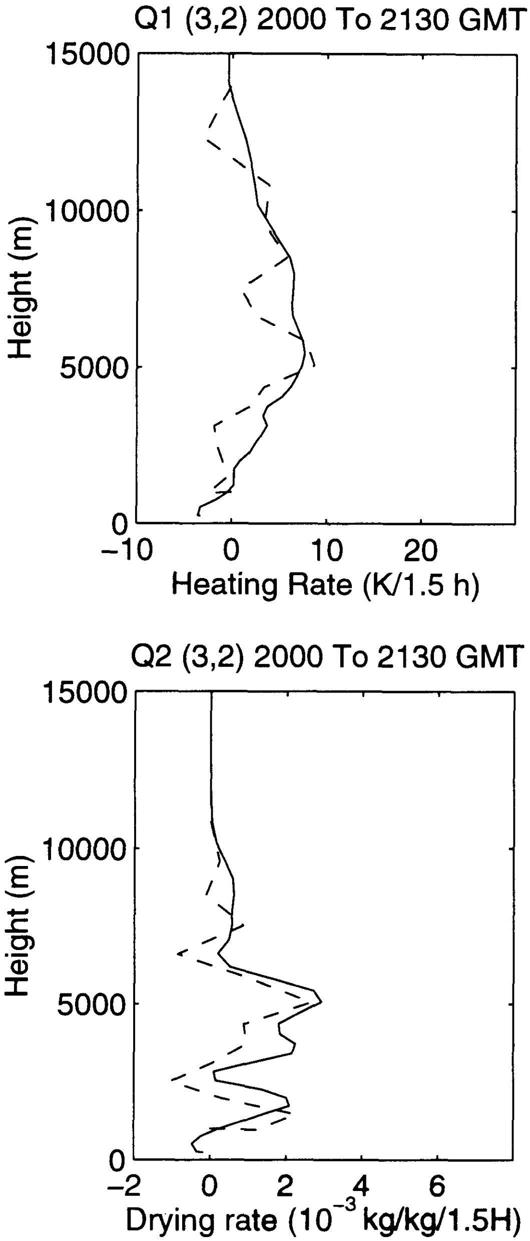


*Fig. 8.* As in Fig. 4 except for a 90-min period, 2000 GMT to 2130 GMT for grid point (3, 2).

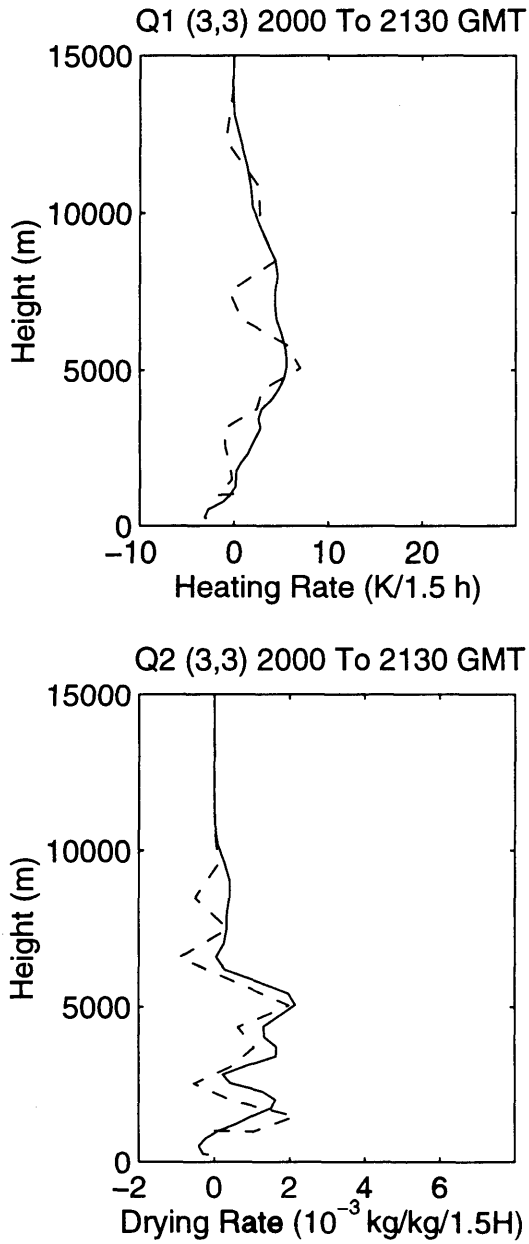


*Fig. 9.* As for Fig. 8 except for grid point (3, 3).

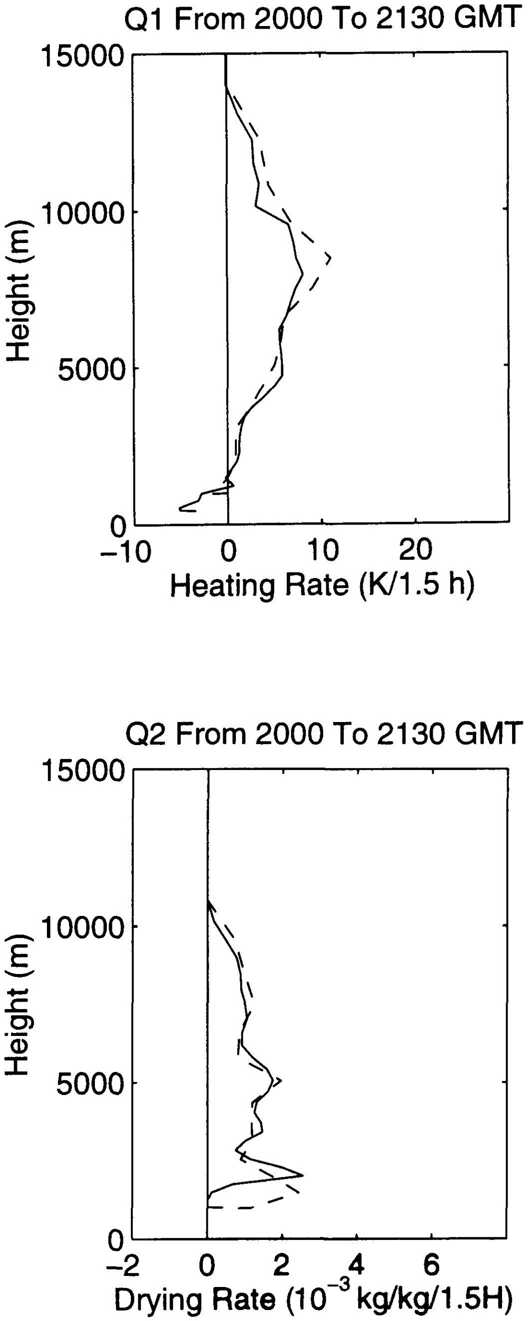


*Fig. 10.* Comparison of averaged (dashed) and CPS diagnosed (solid) $Q_1$ (top) and $Q_2$ (bottom) for a 90-min period, 2000 GMT to 2130 GMT, on 20 May 1979.

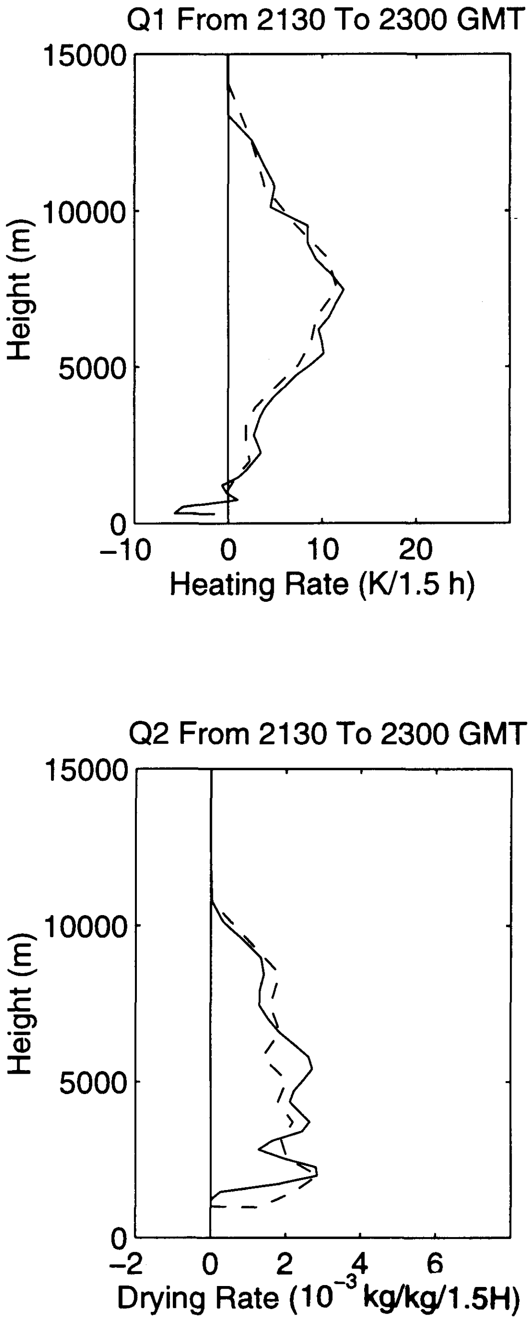


*Fig. 11.* Comparison of averaged (dashed) and CPS diagnosed (solid) $Q_1$ (top) and $Q_2$ (bottom) for a 90-min period, 2130 GMT to 2300 GMT, on 20 May 1979.

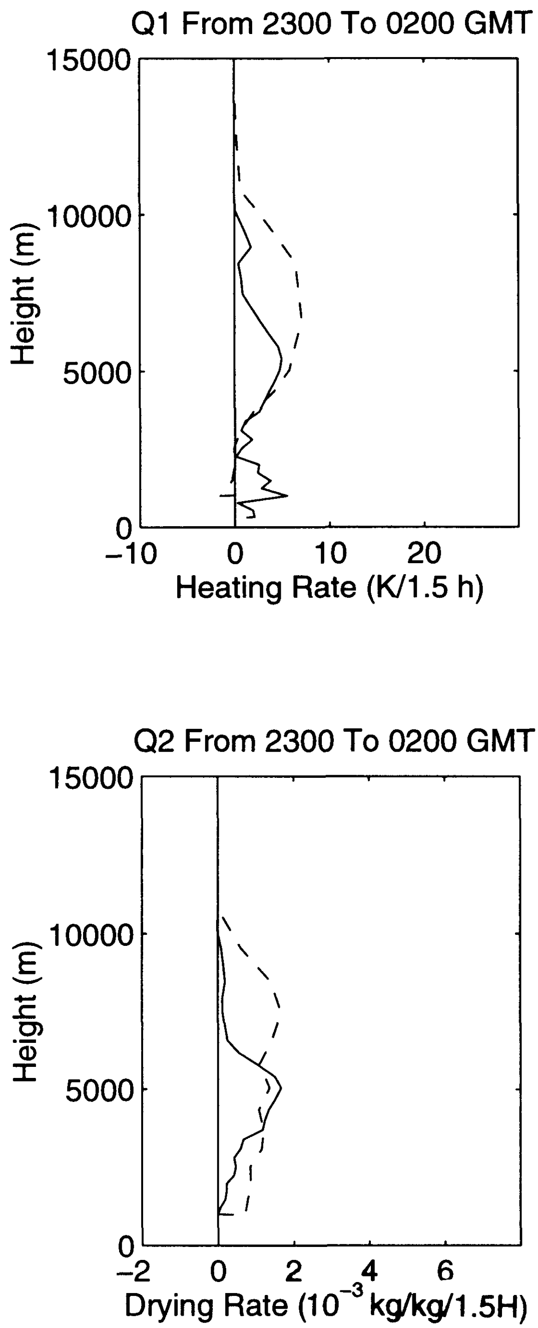


*Fig. 12.* Comparison of averaged (dashed) and CPS diagnosed (solid) $Q_1$ (top) and $Q_2$ (bottom) for a three hour period, 2300 GMT to 0200 GMT, on 21 May–22 May 1979.

the convection. Despite this, the comparisons, especially of $Q_2$ are still good. Previous studies, even though comparing on an average basis, have not diagnosed $Q_2$ very well.

Fig. 11 is as for 10 except that it is for the 2130 GMT to 2300 GMT time period and the area is displaced eastward reflective of the movement of the convective activity. The area represented here is quite close to that designated as box B in Grell et al. (1991). In both amount and vertical structure, the CPS diagnoses are quite similar to the observed values during this time. Watson et al. (1988) noted that the level of convective within their storm scale region remained about the same during this time.

In many MCSs, stratiform rain contributes a significant portion of the latent heating and this greatly complicates evaluation of semi-prognostic comparisons especially when the comparisons are done over an extended time period. Fortunately, this is not the case for the comparisons shown above. After 2300 GMT on 20 May, an increasing and later majority portion of the rainfall in the storm scale region came from stratiform rain. Fig. 12 shows the overall CPS and observation comparisons for the 2300 GMT to 0200 GMT time period on the same basis as Figs. 10 and 11. Again the area considered is quite similar to Grell's box B. During this time, the CPS diagnoses 50% or less of the observed heating and drying which is consistent with the Watson et al. (1988) conclusions that the amounts of convective and stable precipitation were about the same. In addition, the observed level of maximum heating occurs at a higher level than that diagnosed by the CPS; this is consistent with the occurrence of widespread MCS stratiform rainfall that originates in the upper troposphere.

## 4. Summary

A new CPS was introduced, described, and tested. It is based on relating the mass and moisture budgets of a convective system to its counterparts at mesoscale model grid scales. The convective system is assumed to consist of an unknown number of large, medium, and small size clouds whose mass and moisture budgets are related to those of the grid scale in a mesoscale model. As there are three unknown for the number of clouds of each size; but only two constraints, a third condition is necessary to close the problem. This final condition is to assume that a convective system maximizes its rate of heating when integrated over the convective cloud depths.

This cumulus parameterization was tested semi-prognostically using storm scale data collected during the SESAME V experiment. This and the SESAME IV observations constitute unique meso-$\beta$ scale resolution of two quite different MCSs. In addition, when the convection was most intense and widespread within the storm scale area, observations were taken at a 90-min time interval. During this intensively observed time period from 2000 GMT to 2300 GMT on 20 May 1979, very little stratiform rainfall fell within the storm scale area. Thus, the semi-prognostic comparisons are not affected by stratiform rain contributions to the heat and moisture budgets and during this early pre-anvil stage in the MCS development, the neglect of radiation in the $Q_1$ budget is justified. After 2300 GMT, stratiform rainfall within the storm scale domain increased markedly surpassing the convective rainfall after 0200 GMT.

Comparisons between the observed $Q_1$ and $Q_2$ and that diagnosed by the cumulus parameterization were done at every convectively active grid point and are generally good. The comparisons include grid points with both weak and strong convective activity; overall comparisons for two 90-min periods: 2000 GMT to 2130 GMT and 2130 GMT to 2300 GMT were also done. The general comparison either at individual grid points or on an overall basis are encouraging. After 2300 GMT, with stratiform rainfall contributing an increase portion of the latent heating, the average diagnosed $Q_1$ and $Q_2$ values are less than those observed and the heights of the maximum observed heating is positioned at higher levels than that diagnosed by the CPS. The observed heating in the upper troposphere with little or no heating or perhaps even cooling in the lower troposphere is consistent with the development of the MCS as concluded by Watson et al. (1988). As mentioned above, in the development of this CPS, it was assumed that mesoscale areas of ascent such as the anvil in SESAME V will be explicitly resolved and accounted for by grid scale dynamics and microphysics.

The time and space scales of comparison done in this study are unique as all prior semi-prognostic studies have shown $Q_1$ and $Q_2$ comparisons obtained from considerable space and time averaging. This type of averaging is more appropriate when the tested cumulus parameterization is to be used in a general circulation or other large scale numerical model provided that latent heat release of non-convective precipitation and radiation are properly accounted for. For application to meso-$\beta$ scale prediction, however, the appropriate time and space scales are much closer to those used here. Furthermore, as a significant portion of the rain occurring in MCSs may be of stratiform type, averaging $Q_1$ and $Q_2$ over the entire MCS life cycle incorporates a significant and difficult to unravel contribution from stratiform rain. In order to avoid this dilemma, semi-prognostic testing ought to be applied only when and where rain is mainly convective in nature. In addition, these same kind of comparisons ought to be done for a case where the cumulus parameterization is coupled with a mesoscale model that includes explicit grid scale microphysics and mesoscale dynamics. Then the prognostic type of CPS testing (Grell, 1993) could be done. SESAME V offers a very fine detail of observation with which to do this.

## 5. Acknowledgements

We are indebted to Professor Hsiao-Lin Kuo for his considerable advice and encouragement during the course of this research, Henry Fuelberg for sharing his SESAME V analyses with us, Bill Whitson of the Purdue University Computing Center for his help with many recalcitrant magnetic tapes, and the constructive criticism and comments from four anonymous reviewers. We also benefited significantly from advice from Steve Koch and Dayton Vincent, and informative discussions with Leo Donner. Special thanks to Jim Gardner for reviewing the text. This work was supported by NSF Grants ATMS-8611729 and ATMS-8907881 and NASA Grant NGT-50.

## REFERENCES


Alberty, R., Burgess, D. W., Hane, C. E. and Weaver, J. F. 1979. *SESAME 1979 Operations Summary*. NOAA/ERL, Boulder, Colorado, 253 pp.

Anthes, R. A. 1977. A cumulus parameterization scheme utilizing a one-dimensional cloud model. *Mon. Wea. Rev.* **105**, 270–286.

Arakawa, A. and Schubert, W. 1974. Interaction of cumulus cloud ensemble with the large-scale environment. Part I. *J. Atmos. Sci.* **31**, 674–701.

Betts, A. K. 1986. A new convective adjustment scheme (I). Observational and theoretical basis. *Quart. J. Roy. Meteor. Soc.* **112**, 677–692.

Brown, J. M. 1979. Mesoscale unsaturated downdrafts driven by rainfall evaporation. A numerical study. *J. Atmos. Sci.* **36**, 313–338.

Charney, J. G. and Eliassen, A. 1964. On the growth of the hurricane depression. *J. Atmos. Sci.* **21**, 68–75.

Fankhauser, J. C. 1969. Convective processes resolved by a mesoscale rawinsonde network. *J. Appl. Meteor.* **8**, 778–798.

Fankhauser, J. C. 1988. Estimates of thunderstorm precipitation efficiency from field measurements in CCOPE. *Mon. Wea. Rev.* **116**, 663–684.

Foote, G. B. and Fankhauser, J. C. 1973. Airflow and moisture budget beneath an Northeast Colorado hailstorm. *J. Appl. Meteor.* **12**, 1330–1352.

Frank, W. M. 1983. The cumulus parameterization problem. *Mon. Wea. Rev.* **111**, 1859–1871.

Frank, W. M. and Cohen, C. 1987. Simulation of tropical convective systems. Part I. A cumulus parameterization. *J. Atmos. Sci.* **44**, 3787–3799.

Fritsch, J. M. and Chappell, C. F. 1980. Numerical prediction of convectively driven mesoscale pressure systems. Part I. Convective parameterization. *J. Atmos. Sci.* **37**, 1722–1733.

Fuelberg, H. E. and Printy, M. F. 1983. Meso-$\beta$ scale thunderstorm-environment interactions during AVE-SESAME V (20–21 May 1979). *Bull. Amer. Meteor. Soc.* **64**, 1144–1156.

Fuelberg, H. E., Lin, Y.-L. and Chang, H.-W. 1986. A moisture analysis of the meso-$\beta$ scale thunderstorm environment during AVE-SESAME V (20–21 May 1979). *Mon. Wea. Rev.* **114**, 534–545.

Grell, G., Kuo, Y.-H. and Pasch, R. 1991. Semi-prognostic tests of cumulus parameterization schemes in the middle latitudes. *Mon. Wea. Rev.* **119**, 5–31.

Grell, G. 1993. Prognostic evaluation of assumptions used by cumulus parameterizations. *Mon. Wea. Rev.* **121**, 764–787.

Haines, P. A. 1992. *Numerical simulation of a squall line. Tests of a new cumulus parameterization.* Ph.D. dissertation, Purdue Univ., 395 pp.

Haines, P. A. and Sun, W.-Y. 1994. A convective cloud model for use in a cumulus parameterization scheme. *Mon. Wea. Rev.* **122**, 165–182.

Knupp, K. R. 1987. Downdrafts within high plains cumulonimbi. Part I. General kinematic structure. *J. Atmos. Sci.* **44**, 987–1008.

Kreitzberg, C. W. and Perkey, D. J. 1976. Release of potential instability, Part I. A sequential plume model within a hydrostatic primitive equation model. *J. Atmos. Sci.* **33**, 456–475.

Kuo, H.-L. 1965. On formation and intensification of tropical cyclones through latent heat release by cumulus convection. *J. Atmos. Sci.* **22**, 40–63.

Kuo, H.-L. 1974. Further studies of the parameterization of the influence of cumulus convection on large-scale flow. *J. Atmos. Sci.* **31**, 1232–1240.

Kuo, Y.-H. and Anthes, R. A. 1984. Semiprognostic tests of Kuo-type cumulus parameterization schemes in an extratropical convective system. *Mon. Wea. Rev.* **112**, 1498–1509.

Marwitz, J. D. 1972. Precipitation efficiency of thunderstorms on the high plains. *J. Res. Atmos.* **6**, 367–370.

McNab, A. L. and Betts, A. K. 1978. A mesoscale budget study of cumulus convection. *Mon. Wea. Rev.* **106**, 764–778.

Molinari, J. and Corsetti, T. 1985. Incorporation of cloud-scale and mesoscale downdrafts into a cumulus parameterization. Results of one- and three-dimensional integrations. *Mon. Wea. Rev.* **113**, 485–501.

Molinari, J. and Dudek, M. 1992. Parameterization of convective precipitation in mesoscale numerical models. A critical review. *Mon. Wea. Rev.* **120**, 326–344.

Ogura, Y. and Chen, Y. 1977. A life history of an intense mesoscale convective storm in Oklahoma. *J. Atmos. Sci.* **34**, 1458–1476.

Ooyama, K. V. 1971. A theory on parameterization of cumulus convection. *J. Meteor. Soc. Japan* **49**, 369–379.

Schlesinger, R. E. 1990. Feedback of deep moist convection to its near environment as diagnosed from three-dimensional numerical model output. Results from an early experiment. *J. Atmos. Sci.* **47**, 1390–1412.

Schlesinger, R. E. 1994. Heat, moisture, and momentum budgets of isolated deep midlatitude and tropical convective clouds as diagnosed from three-dimensional model output. Part I. Control experiments. *J. Atmos. Sci.* **51**, 3649–3673.

Song, J. L. and Pielke, R. A. 1987. The influence of deep cumulus convection on sea breeze dynamics over south Florida. Part I. Model development. *Atmospheric Science Paper no. 426*, Colorado State Univ. 45 pp.

Soong, S.-T. and Ogura, Y. 1977. A determination of the trade-wind cumuli population using BOMEX data and an axisymmetric cloud model. *J. Atmos. Sci.* **33**, 992–1007.

Sun, W.-Y. 1984. Rainbands and symmetric instability. *J. Atmos. Sci.* **41**, 3412–3426.

Sun, W.-Y. and Chern, J.-D. 1993. Diurnal variation of lee vortices in Taiwan and the surrounding area. *J. Atmos. Sci.* **50**, 3404–3430.

Sun, W.-Y. and Chern, J.-D. 1994. Numerical experiments of vortices in the wake of large mountains. *J. Atmos. Sci.* **51**, 191–209.

Tiedtke, M. 1989. A comprehensive mass flux scheme for cumulus parameterization in large-scale models. *Mon. Wea. Rev.* **117**, 1779–1800.

Watson, A. I., Meitin, J. G. and Cunning, J. B. 1988. Evolution of the kinematic structure and precipitation characteristics of a mesoscale convective system on 20 May 1979. *Mon. Wea. Rev.* **116**, 1555–1567.

Weissbluth, M. J. and Cotton, W. R. 1993. The representation of convection in mesoscale models. Part I. Scheme fabrication and calibration. *J. Atmos. Sci.* **50**, 3852–3872.

Yanai, M., Esbensen, S. and Chu, J.-H. 1973. Determination of bulk properties of tropical cloud clusters from large-scale heat and moisture budgets. *J. Atmos. Sci.* **30**, 611–627.

Zhang, D.-L. and Fritsch, J. M. 1986. Numerical simulation of the meso-$\beta$ scale structure and evolution of the 1977 Johnstown flood. Part I. Model description and verification. *J. Atmos. Sci.* **43**, 1913–1943.

Zhang, D.-L. and Gao, K. 1989. Numerical simulation of an intense squall line during 10–11 June 1985 PRE-STORM. Part II. Rear inflow, surface pressure perturbations and stratiform precipitation. *Mon. Wea. Rev.* **117**, 2067–2094.

Zipser, E. J. and LeMone, M. A. 1980. Cumulonimbus vertical velocity events in GATE. Part II. Synthesis and model core structure. *J. Atmos. Sci.* **37**, 2458–2469.



Tellus A/48/2-7